Published in Philosophical Magazine,
Vol. 34, No. 6, 1169-1184 (1976)

LBL-3142

COMPUTER SIMULATION OF THE CONTRAST OF SMALL DISLOCATION LOOPS IN FIELD-ION IMAGES OF F.C.C. CRYSTALS

Kaj Stolt and Jack Washburn

August 27, 1976

Prepared for the U. S. Energy Research and
Development Administration under Contract W-7405-ENG-48

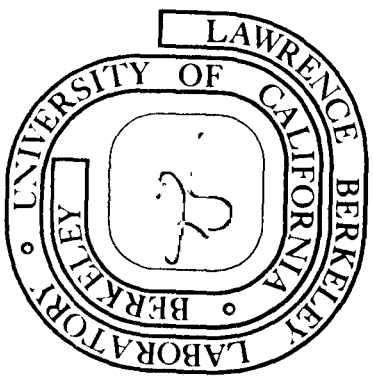

LBL-3142

DISCLAIMER

PHILOSOPHICAL MAGAZINE, 1976, VOL. 34, NO. 6, 1169–1184

Computer simulation of the contrast of small dislocation loops in field-ion images of f.c.c. crystals

By KAJ STOLT† and JACK WASHBURN

Department of Materials Science and Engineering, University of California, and Materials and Molecular Research Division, Lawrence Berkeley Laboratory, University of California, Berkeley, California 94720, U.S.A.

[Received 30 June 1975 and in final form 27 August 1976]

ABSTRACT

It is shown that small dislocation loops of diameter 30 Å or less cause field-ion image contrast while wholly inside the tip. During a field-evaporation sequence that brings the loop successively closer to the surface, characteristic changes in the contrast occur which make it possible to distinguish between vacancy-type and interstitial-type loops. For a single photograph, however, unambiguous interpretation of the image contrast observed is not possible for small loops. The contrast effects for small loops are in many cases rather slight distortions of the image rings and, for a single photograph, could occur for other reasons such as tip asymmetry or the presence of impurities. For this reason an entire field-evaporation sequence is essential. It is pointed out that only sessile loops can be observed in the FIM, since the stresses associated with the electric field will remove glissile loops from the specimen.

§ 1. INTRODUCTION

The shell model of Moore (1962) and the $\mathbf{g} \cdot \mathbf{b}$ criterion of Pashley (1965) and Ranganathan (1966) have been applied with considerable success to the prediction of the field-ion contrast of dislocated crystals (for reviews see Bowkett and Smith (1970) and Stolt (1973))‡. The realization that a dislocation loop intersecting the surface of a field-ion tip will appear as a dislocation dipole has allowed the contrast of dislocation loops to be worked out either intuitively (Smith, Fortes, Kelly and Ralph 1968, Smith, Morgan and Ralph 1968) or by computer simulation (Sanwald and Hren 1968, Perry and Brandon 1968 a, b). The following nomenclature has come into use to describe the image contrast of dislocations (Smith, Fortes, Kelly and Ralph 1968, Smith, Morgan and Ralph 1968): for perfect dislocations $\mathbf{g} \cdot \mathbf{b} = p$ (always an integer) gives the number of leaves in the image spiral, and for partial dislocations $\mathbf{g} \cdot \mathbf{b}_p = q$ gives the size of the step by which plane edges are separated as they cross the fault associated with the partial.

The problem of correctly identifying dislocation loops based on their contrast in field-ion images remains largely unsolved, however. This is

† Now at Coordinated Science Laboratory, University of Illinois, Urbana, Illinois 61801, U.S.A.

‡ $\mathbf{g}$ is the reciprocal lattice vector corresponding to the pole of interest and $\mathbf{b}$ is the Burgers vector of the dislocation.

especially the case for small loops. In this respect the work of Fortes (1970) was a promising start. He worked out a method of distinguishing between the faulted loops in f.c.c. crystals (intrinsic and extrinsic Frank or Shockley loops) based on the determination of $|q|$ or $|p|$ and the plane of the loop from the image. The choice is not always unequivocal since different loops may yield the same value of $|q|$ or $|p|$, and for small loops the method breaks down since $|q|$ or $|p|$ values cannot be obtained at all. A loop will be considered small for the purpose of this discussion if, during field evaporation, it intersects only one plane edge at a time. If this is the case it is not possible to tell whether $|q|$ is smaller or greater than unity or even whether $\mathbf{g} \cdot \mathbf{b}$ is integral or non-integral. Since, in a typical field-ion tip, second and third ledge widths of up to 20 Å are quite common and since a dislocation loop will only rarely intersect the plane edges at right angles, this situation may often arise with loops as large as 30 Å emerging close to low-index poles.

This computer study extends the prediction of dislocation-loop contrast to such small loops in f.c.c. crystals. Only prismatic loops†, either faulted (Frank) or perfect, are considered. Although observations of glide loops have been reported (Fortes and Ralph 1968), the present authors find the concept of stable glide loops unrealistic on physical grounds which will be detailed in the Discussion (§ 4). However, since a perfect prismatic loop can be stretched out along its glide cylinder into a configuration that closely resembles a glide loop, the contrast of glide loops is simulated with this case in mind.

§ 2. The computer model

2.1. *The displacement field*

The displacement field of a closed dislocation loop is given by Hirth and Lothe (1968, p. 96) in the following form :

$$\mathbf{u}(\mathbf{r}) = \frac{\mathbf{b}}{4\pi} \int_A \frac{\mathbf{R} \cdot d\mathbf{A}'}{R^3} - \frac{1}{4\pi} \oint_C \frac{\mathbf{b} \times d\mathbf{l}'}{R} + \frac{1}{8\pi(1-\nu)} \operatorname{grad} \oint_C \frac{(\mathbf{b} \times \mathbf{R}) \cdot d\mathbf{l}'}{R}. \qquad (1)$$

Here $\mathbf{b}$ is the Burgers vector of the loop, $d\mathbf{l}'$ the differential line element of the dislocation line C, and $d\mathbf{A}'$ the surface element of the cut surface. $\mathbf{R} = \mathbf{r}' - \mathbf{r}$, where $\mathbf{r}$ is the position vector of the point for which the displacement is computed, and $\mathbf{r}'$ is the position vector of the line element $d\mathbf{l}'$. Poisson's ratio ν is given the value $\frac{1}{3}$ in these calculations. The displacement field, $\mathbf{u}(\mathbf{r})$, of any specific loop is obtained by carrying out the integrations in eqn. (1) over the loop.

2.2. *Shape of loops*

The loops are taken to be regular hexagons. This shape is chosen for computational convenience, but is also physically plausible for Frank loops on the {111} planes of the f.c.c. lattice. The displacements are worked out in a coordinate system centred on the loop as in fig. 1 (*a*), which shows one

† For the purpose of this paper, a ' glide loop ' is defined as a loop with Burgers vector in the plane of the loop. All other loops will be referred to as ' prismatic loops '. Prismatic loops may be either perfect or imperfect.

Fig. 1

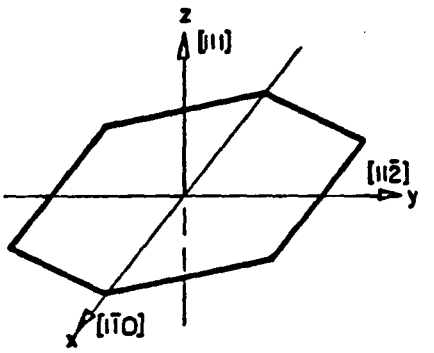

(*a*)

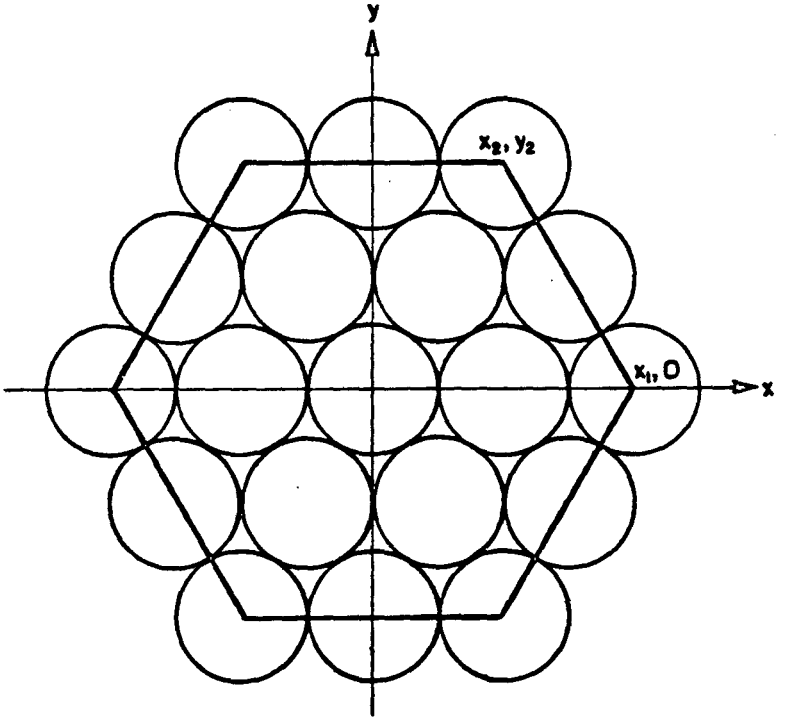

(*b*)

(*a*) Coordinate system used to calculate the displacement field of a hexagonal loop.
(*b*) Illustration of ' five-atom loop '.

possible set of axes. The parameters used to describe a loop are defined in fig. 1 (*b*). For the regular hexagon $x_1 = 2x_2$ and $y_2 = \sqrt{3}x_2$. The size of a loop will be specified by the number of atoms contained along its diagonal. Thus the loop in fig. 1 (*b*) is a 'five-atom loop'. For the hexagonal loop the line integrals in eqn. (1) can be solved analytically, using elementary functions. The surface integral can be integrated analytically only once, however. The second integration is performed numerically in the computer programme, using the Romberg algorithm (Ralston 1965), which in this case achieves an accuracy of one part in 1000 with only a few iterations. An expression for the displacement of a lattice point is thus obtained in terms of its coordinates (x, y, z) relative to the centre of the loop and of the size (x_2) of the loop.

2.3. *Lattice model*

The f.c.c. space lattice is built up by stacking (111) planes in proper sequence. This choice of basis facilitates the introduction of loops on (111). The lattice coordinate system coincides (in orientation) with that of the loops. A dislocation loop is positioned in the lattice by specifying the coordinates of its centre in lattice coordinates. The shell criterion is applied in the normal manner after the displacements of eqn. (1) have been imposed on the crystal. The vacancies comprising a vacancy loop must be removed from the lattice, i.e. the computer is instructed to omit the corresponding lattice points. For interstitial loops the disc of interstitials is introduced bodily into the lattice in the correct position.

2.4. *Simulated field evaporation*

Evaporation sequences are simulated by increasing the radius of the tip by ΔR between plots, while moving the centre of the shell down the z-axis by $\Delta z > \Delta R$. This method corresponds closely to actual field evaporation (Stolt 1973).

2.5. *Surface relaxation*

In a field-ion tip, if a dislocation loop is to be observed, it must be close to the surface of the crystal. The proximity of the surface will, of course, affect the displacement field of the loop. In previous work the effect of surface relaxation has been ignored, no doubt due to the complexity of the problem. The effect of the surface on the displacement field can be evaluated to a first approximation by superposing, on the displacement field of the loop, the displacement field of a mirror loop of the opposite kind to the actual loop, i.e. with opposite Burgers vector and reflected in the plane of the surface (Hirth and Lothe 1968, p. 130). Figure 2 shows the simulated field-ion contrast of a Frank interstitial loop on (111) below (110), for which configuration $|q| = 4/3$. In fig. 2 (*a*)–(*c*) loop displacements alone were used, and in fig. 2 (*d*)–(*f*) the mirror-loop displacements were superposed. A $|q|$ value of 4/3 could be deduced from fig. 2 (*a*) but hardly from any of the other plots. Where the mirror-image loop was used $|q|$ appears to be close to 2. Since the effect of the mirror loop is realistic, although possibly exaggerated, it appears that the **g . b** criterion is not quantitatively precise at the surface.

Fig. 2

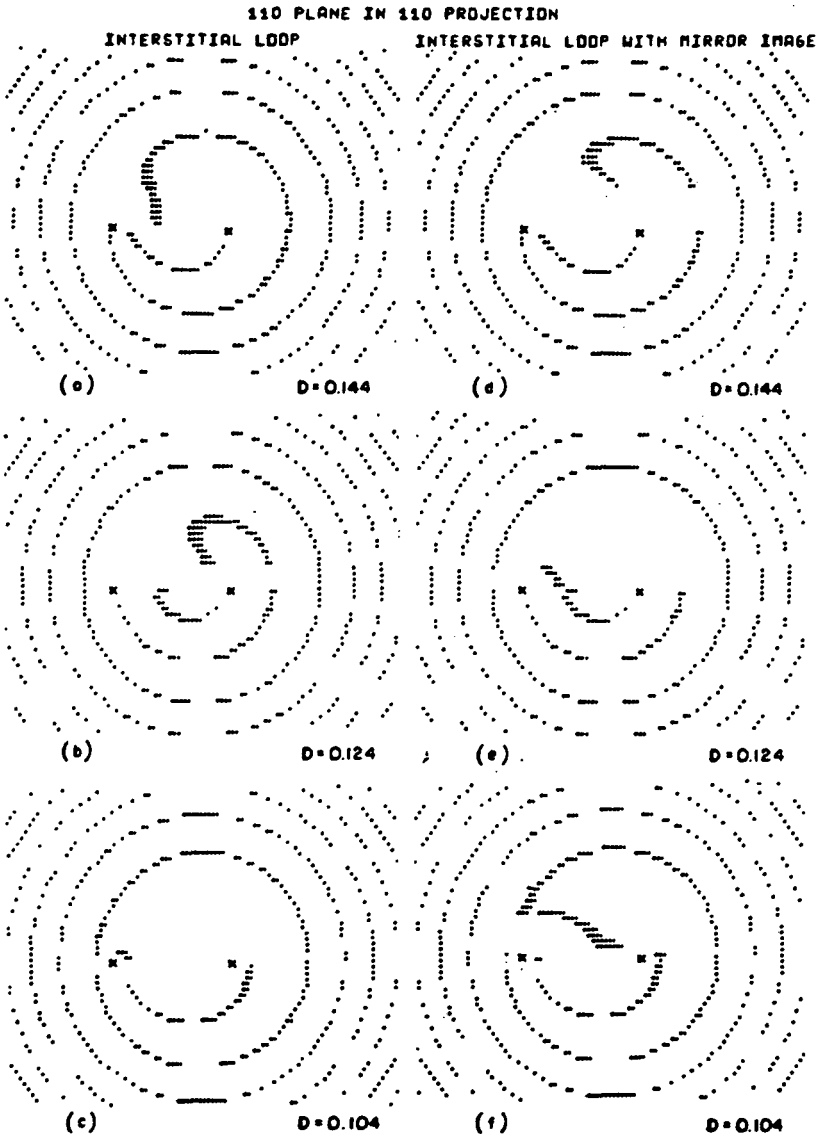

Illustration of the effect of adding image-loop displacements. Interstitial loop on (111) emerging on the (110) plane. The points of emergence of the partial dislocations are marked X. D is defined in fig. 4. Tip radius 375 lattice constants. Thirty-one-atom loops.

In all cases where the mirror-loop model was applied it was found only to enhance qualitative contrast characteristics which could be demonstrated with the simple model using loop displacement alone (Stolt 1973). Therefore, the simple model, with no mirror-image loop, has been used in the rest of this work.

§ 3. Results

3.1. *Frank loops*

The difference in simulated contrast between Frank loops of vacancy and interstitial types is most obvious while the loops are wholly beneath the surface of the tip. Figure 3 shows 13-atom loops (~30 Å in Pt) on (111)

Fig. 3

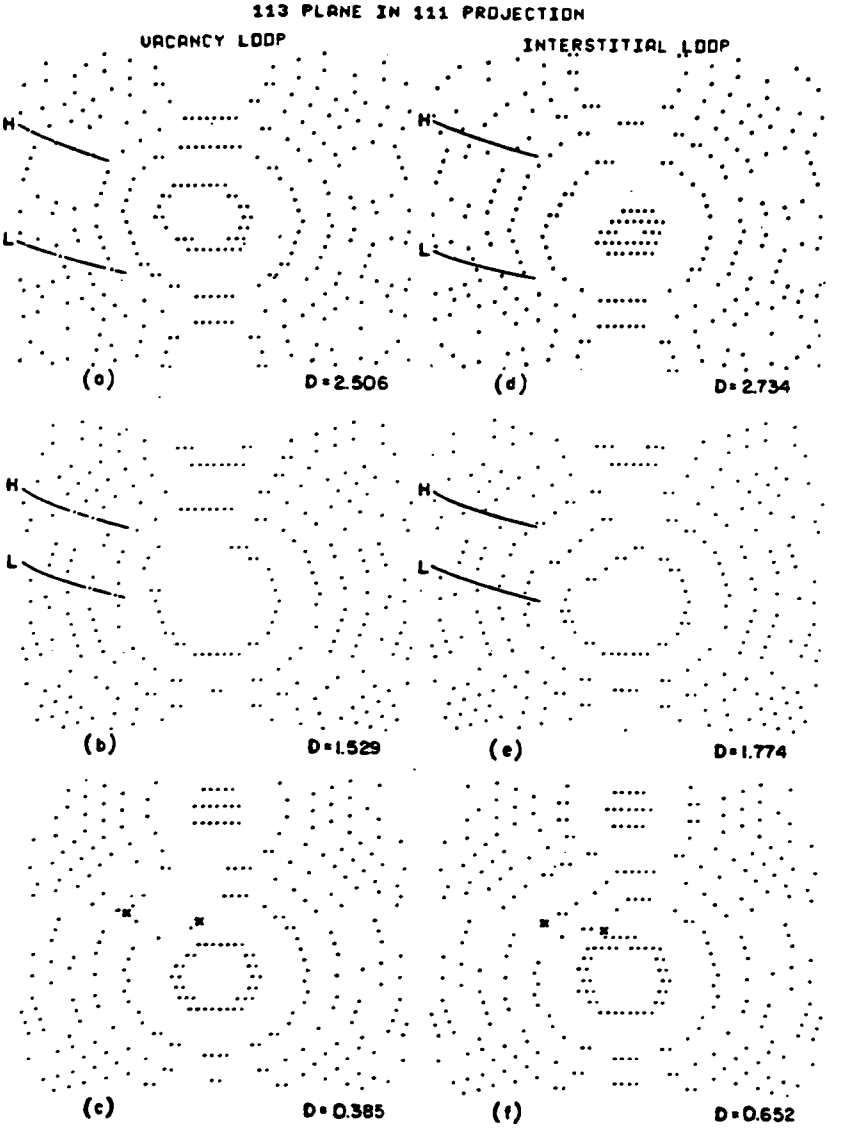

Comparison of the contrast caused by a Frank vacancy loop (*a*, *b*, *c*) and a Frank interstitial loop (*d*, *e*, *f*) when ϕ is small. ϕ, H, L and D are defined in fig. 4. Both loops are on the (111) plane and emerge on the (113) plane. The points of emergence of the dislocations are marked X. (See text for discussion.) Tip radius 98 lattice constants. Thirteen-atom loops.

under (113), which first became noticeable when their distance beneath the surface was about five loop radii (Stolt 1973). Three rather widely separated stages of long field-evaporation sequences through a vacancy loop and an interstitial loop are shown. L is the trace of the plane of the loop in the surface and H indicates the position where the normal to the loop through its centre intersects the surface (see fig. 4). While the loops are beneath the

Fig. 4

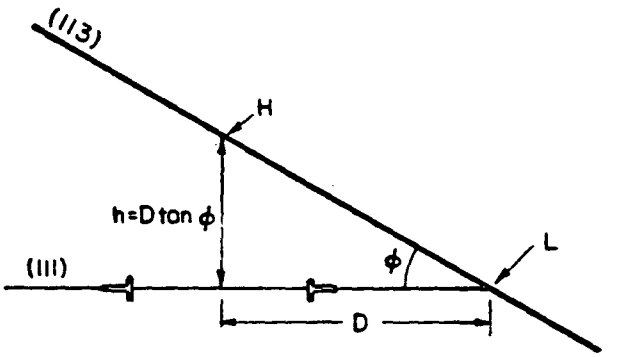

Definition of symbols used to indicate the location of a loop wholly beneath the surface. H = intersection of loop normal with surface. L = intersection of loop plane with surface. D = distance of loop centre from surface measured in units of the loop radius. ϕ = angle between loop plane and surface plane.

surface, the vacancy loop is seen to cause the (113) plane edges to stretch towards or through the depression of the surface above the loop, whereas the influence of the interstitial loop is to bend the plane edges towards the centre of the pole, eventually developing a kink in one or two rings. This difference is quite distinct and makes it possible to infer the nature of a Frank loop by inspection. This contrast effect is quite general and is not restricted to the (113) pole nor to cases where the angle between loop plane and surface is small. Loops on (111) under (11$\bar{1}$) ($\phi \simeq 70°$) can be distinguished by this effect as illustrated in figs. 5 (*a*) and (*b*), although the effect here is rather subtle. In this case the loops have to be closer to the surface to cause contrast. Loops emerging further away from low-index poles will also cause similar contrast, although the bending of the rings is harder to detect where the ledge width is small (Stolt 1973).

When the surface intersects the loops, as in figs. 3 (*c*) and (*f*), the difference between vacancy and interstitial loop contrast is no longer so obvious. If the crosses marking the emergence of the dislocations in these plots were removed it would be rather hard to infer the cause of the contrast, and especially to infer a $|q|$—value of 5/3 ($\mathbf{b} = 1/3[111]$, $\mathbf{g} = [113]$). This is not of great importance since further field evaporation would clarify the matter. Loop characterization must, in fact, be based on a field-evaporation sequence, special care being taken to record that part of the sequence which occurred while the loop was still wholly inside the tip.

Fig. 5

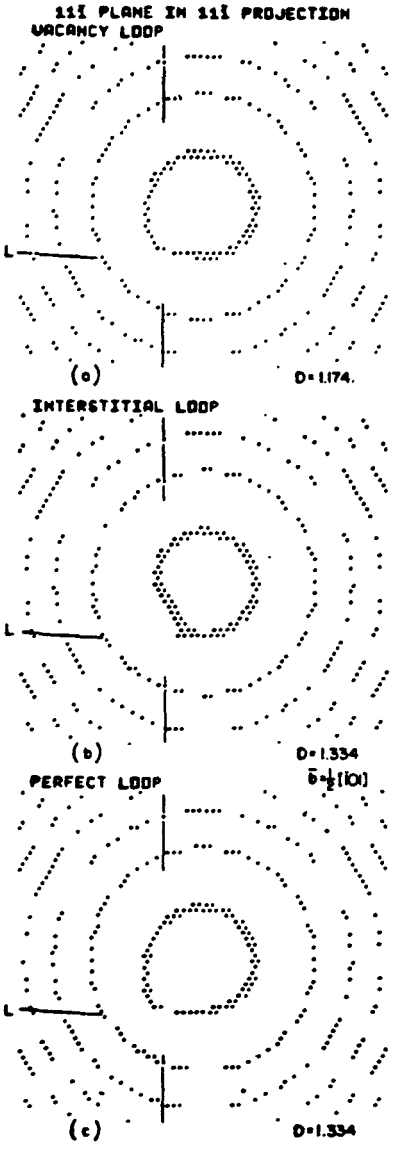

Comparison of the contrast caused by a Frank vacancy loop (*a*), a Frank interstitial loop (*b*) and a perfect glide loop (*c*) when ϕ is large. All loops are on the (111) plane beneath the (11$\bar{1}$) plane. ϕ, L and D are defined in fig. 4. (See text for discussion.) Tip radius 100 lattice constants. Eleven-atom loops.

It is not necessary to determine the plane of the loop in order to correctly identify vacancy and interstitial loops by the contrast effects illustrated in figs. 3 and 5. Considering a pole under which two {111} planes are in equivalent positions, such as (111) and (11$\bar{1}$) under (110), it is realized first that

an interstitial loop, say, on (111) above the (110) pole is exactly equivalent to an interstitial loop on (11$\bar{1}$) below the pole. The contrast effects in these two cases would be mirror images. Since according to figs. 3 and 5 loops on (111) cause the same type of contrast whether above or below the pole, it follows that loops of the same type would cause the same type of contrast whether on (111) or (11$\bar{1}$) on the same side of the pole (Stolt 1973).

3.2. *Perfect prismatic loops*

Frank loops and perfect prismatic loops represent similar physical configurations, and will consequently have similar displacement fields associated with them.

This statement is, however, true only so long as the perfect loop stays on, or close to, the {111} plane on which it was formed. With a shear stress acting along the glide cylinder of the prismatic loop, the loop will be rotated and stretched out along the glide cylinder. In the extreme case the prismatic perfect loop will approach a long, outstretched loop on one of the {111} planes containing its Burgers vector. A perfect prismatic loop formed on (111), with Burgers vector $\frac{1}{2}$[110], for instance, is glissile on the cylinder formed by ($\bar{1}$11) and (1$\bar{1}$1). When sufficiently stretched out along the cylinder this loop becomes a dislocation dipole.

The stress distribution in a field-ion tip is not known exactly, but calculations (Smith, Birdseye and Goringe 1973) indicate that high shear stresses will be present in certain regions of the tip. The resolved shear stress on a plane is a function of its position in the tip as well as of its orientation. It is thus possible for some planes to experience high resolved shear stresses and others to be virtually stress-free. For the purpose of this section it is noted that, under these conditions, perfect prismatic loops may stay on or near their {111} plane of formation or rotate towards the edge orientation, {110}, or alternatively they may be stretched out as described above until their configuration approaches that of a screw dipole. In order to study the first case, the field-ion contrast of a perfect loop will be simulated using a hexagonal loop on (111) with Burgers vector $\frac{1}{2}$[110]. For the second case it will be simulated using a glissile hexagonal loop on (111) with Burgers vector $\frac{1}{2}$[$\bar{1}$01]; this model should be quite adequate since contrast will be caused almost entirely by that part of the loop which is close to the surface.

A $\frac{1}{2}$[110] prismatic loop on (111) closely resembles a Frank loop and should cause similar contrast. This is clearly borne out by computer simulation, as illustrated in figs. 6 (*a*)–(*c*). In these plots the perfect prismatic loop of vacancy type is in exactly the same position as the Frank vacancy loops in figs. 3 (*a*)–(*c*). The similarity of the two patterns is striking, so that a distinction between perfect prismatic loops and Frank loops is not possible on simple inspection of the contrast. The distinction must be based on the $\mathbf{g} \cdot \mathbf{b}$ criterion. If the loop is large enough to make this meaningful, and if the $\mathbf{g}$ $\mathbf{b}$ values are different for the two types of loop, the distinction should usually be possible. In the cases illustrated in fig. 3 and fig. 6, for instance, $|q| = 5/3$ for the Frank loop, and $|p| = 1$ for the perfect loop.

Figures 6 (*d*)–(*f*) show the corresponding field-evaporation stages for the $\frac{1}{2}$[$\bar{1}$01] loop. In this case the contrast is a little weaker in the sense that the

Fig. 6

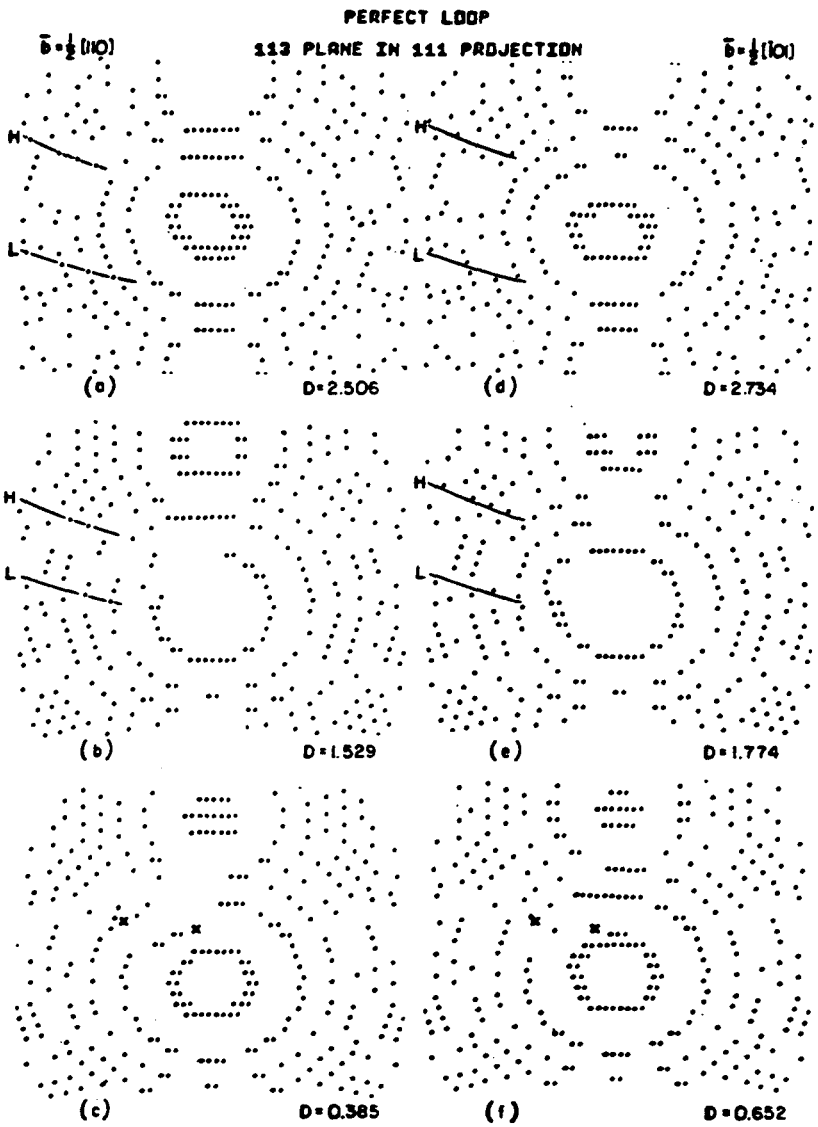

Comparison of the contrast caused by a perfect prismatic loop (*a*, *b*, *c*) and a perfect glide loop (*d*, *e*, *f*) when ϕ is small. ϕ, H, L and D are defined in fig. 4. Both loops are on the (111) plane and emerge on the (113) plane. The points of emergence of the dislocations are marked X. (See text for discussion.) Tip radius 98 lattice constants. Thirteen-atom loops.

loop must be closer to the surface to be visible. This is evident on comparing figs. 6 (*a*) and (*d*). The contrast is, however, qualitatively the same, as is seen on comparing fig. 6 (*a*) (or fig. 3 (*a*)) with fig. 6 (*e*). There is thus no obvious qualitative difference on which to base a distinction between these two cases. It should, however, be noted that in fig. 3 and fig. 6 (*a*)–(*c*) the

(112) plane edges are distorted by the presence of the loop under (113). In figs. 3 (*b*) and 6 (*b*) the second (112) image ring is stretched towards the loop, whereas the third (112) image ring in fig. 3 (*e*) is slightly bent towards the centre of the (112) pole directly above the loop. This effect is clearly visible in figs. 3 (*c*), (*f*) and 6 (*c*). No such effect is seen in figs. 6 (*d*)–(*f*). Although this case is admittedly somewhat special in that the loop is positioned between

Fig. 7

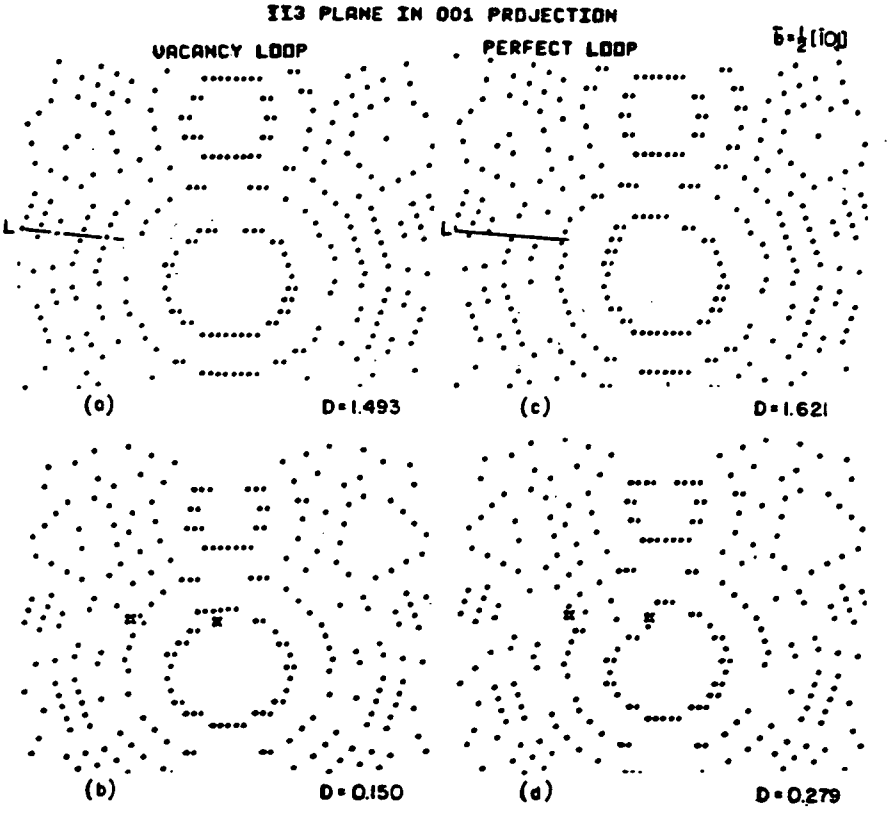

Comparison of the contrast caused by a Frank vacancy loop (*a*, *b*) and a perfect glide loop (*c*, *d*) when ϕ is large. ϕ, L and D are defined in fig. 4. Both loops are on the (111) plane and emerge on the ($\bar{1}\bar{1}3$) plane. The points of emergence of the dislocations are marked X. (See text for discussion.) Tip radius 95 lattice constants. Thirteen-atom loops.

the (113) and (112) poles, the effect noted above is simply a consequence of the basic difference between the displacement fields of Frank loops and glide loops. The contrast of a Frank loop will in most cases be visible far above the intersection of the loop plane with the surface. The only exception to this rule occurs when a Frank loop is nearly at right angles to the surface. This is demonstrated in fig. 7 for loops on (111) under ($\bar{1}\bar{1}3$) ($\phi \simeq 80°$). In this case the Frank vacancy loop is hardly noticeable until it is intersected

Fig. 8

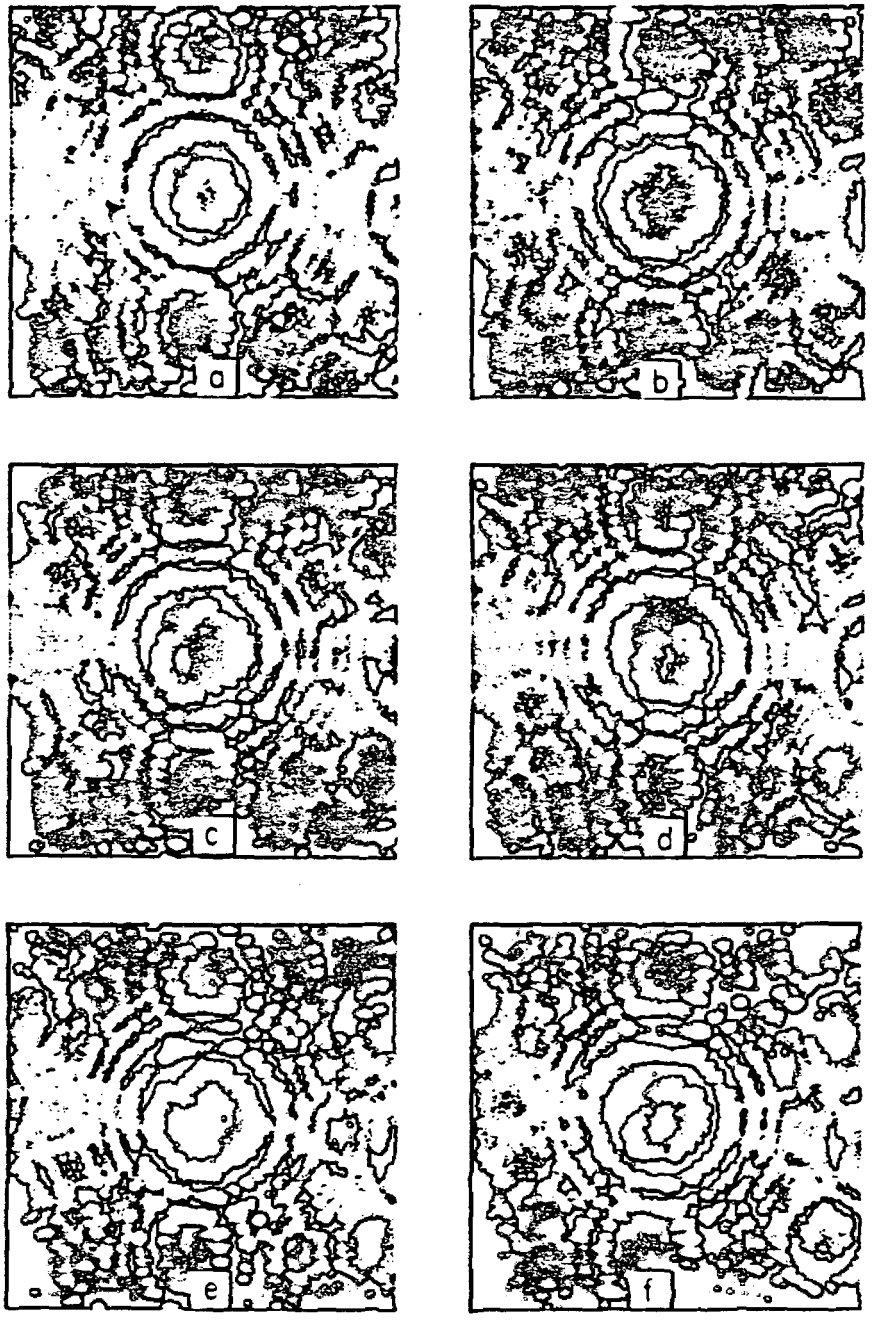

Field-ion micrographs of (110) plane of Ir crystal. Six stages of evaporation sequence show contrast typical of small interstitial loop.

by the surface, whereas the perfect glissile loop with Burgers vector $\frac{1}{2}[\bar{1}01]$ causes contrast when it is about one loop radius below the surface ($|p|=2$ for this loop). For neither loop is there any noticeable effect on the $(\bar{1}\bar{1}5)$ plane edges {$(\bar{1}\bar{1}5)$ is the well developed pole above $(\bar{1}\bar{1}3)$} until the surface intersects the loop and then only on those image rings actually cut by the loops, such as the third $(\bar{1}\bar{1}5)$ ring in fig. 7 (*d*). In this connection comparison with the plots in fig. 5, for which $\phi \simeq 70°$, is of interest.

The observations made in this section may be briefly summarized as follows. Prismatic loops will cause contrast in parts of the surface located above the intersection of loop plane and surface. Glide loops, on the other hand, will cause contrast only close to this intersection. The features of the contrast discussed in connection with figs. 5, 6 and 7 are merely the geometrical consequences of this fact. On the basis of these computer simulations and in the light of their experience with experimental images, the authors do not consider that these effects are strong enough always to permit a distinction between prismatic and glide loops. These effects are sometimes helpful, however, and should be taken into account. If, for instance, a loop in the position of the loop in fig. 3 is not observed to bend the (112) plane edges it is unlikely to be a prismatic loop on (111).

3.3. *Experimental observations*

Figure 8 shows the (110) region of an ion-bombarded Ir specimen (Stolt 1973). Six stages of an evaporation sequence are displayed, showing the type of contrast predicted for small interstitial loops (fig. 3). This behaviour persisted during the removal of seven (110) planes. These micrographs are included here to indicate that the type of contrast predicted by the computer has been observed. It is not quite clear, however, that the contrast in fig. 8 could have been caused only by a dislocation loop (see § 4).

§ 4. Discussion

The main conclusions of this study, i.e. that small dislocation loops cause observable field-ion contrast while wholly inside the tip, that loops of vacancy and interstitial types always cause qualitatively different contrast and that a distinction between glide and prismatic loops can sometimes be made by examining qualitative image features alone, are not based only on the few plots presented here. In particular, the difference between vacancy and interstitial loop contrast is based on a large number of plots with loops in various positions (Stolt 1973). In assessing the validity of these conclusions it should be noted first that they all depend on the long-range strain field of dislocation loops. It is therefore permissible to draw these conclusions from results based on eqn. (1) since this is valid for regions further away from the dislocation line than, say, five atomic diameters. No conclusions are based on the atomic configuration close to the dislocation line.

Equation (1) is derived for a dislocation loop in an infinite elastic continuum, whereas a field-ion tip is of rather limited size. It is intuitively expected that the proximity of the surface will enhance the loop displacements and hence also enhance the contrast effects considered here. This was

shown (§ 2.5) by using a mirror-image model to simulate the effect of the surface. Although the mirror-loop model is by no means analytically rigorous, it is realistic, in the sense that its effect is in the right direction. It might be equally satisfactory simply to multiply the real loop displacements by a factor >1. For the problem of loop identification an exact treatment, or even recognition, of surface relaxation does not appear to be crucial. Surface relaxation is, however, a strong effect and should be taken into account in a quantitative image theory.

A difficulty with previous computer simulations of dislocation-loop contrast is automatically avoided by the use of eqn. (1). It has been pointed out (Ranganathan 1969 a, Ranganathan and Durairaghavan 1969) that the displacement equations for a dislocation dipole must be modified so that the discontinuity of displacement occurs across the loop plane. This feature is already included in eqn. (1). In a computer simulation of Frank-loop contrast by Son and Hren (1970) this precaution appears to have been neglected. In figs. 4 (*a*) and (*b*) of Son and Hren (1970) the configuration is a Frank loop on the (111) plane emerging on the (220) pole, for which case $q=4/3$. The plots, however, represent a case with $|q|<1$ (compare fig. 4 (*b*) of Son and Hren (1970) with figs. 2 (*a*) and (*b*) of this paper). In figs. 5 (*b*) and (*c*) of Son and Hren (1970) the contrast of $\frac{1}{3}$[111] Frank loops of interstitial and vacancy types, respectively, emerging close to the (002) pole, is simulated. In these plots no steps appear in the (002) plane edges crossing the fault although $q=2/3$; instead, distortions appear in other parts of the image. The same problem is also clearly evident in fig. 4 (*b*) of Newman and Hren (1971). An error of this nature in a paper by Hren (1969) has previously been pointed out by Ranganathan (1969 a).

Ranganathan (1969 a, b) has demonstrated that the extra plane corresponding to the fault in an extrinsic stacking fault is visible in the field-ion image. In some of the plots of interstitial loops in the present paper (figs. 2 (*b*), (*e*), (*f*) and 3 (*f*)) the disc of interstitials is also partly visible. This happens rather rarely, however, and thus appears not to be an important feature.

In the authors' opinion even a rather crude approximation to eqn. (1) would yield roughly the same results as are reported here with respect to subsurface loops. This belief is based on actual simulation using simple approximate strain fields, as well as on intuition in retrospect. While it is gratifying that these results are not very sensitive to the choice of model for the strain field, this fact points to another problem. It may be that, although the difference between the contrast of small vacancy and interstitial loops is quite clear, the real difficulty is to be sure that an observed contrast is in fact caused by a dislocation loop, and is not due to some other disturbance of the lattice. The remedy is the detailed recording of a sufficiently long evaporation sequence.

The second component of the model used here, i.e. the shell model, has been used successfully in the past to predict images of faulted crystals. However, some problems which arise in using the shell model are evident in some of the plots in this paper. In figs. 2 (*b*) and (*d*), for instance, there is a gap in the second image ring where it circles around the right side of the loop. Similarly there is a gap in the first ring in figs. 3 (*b*) and 6 (*b*) where this ring

stretches around the surface depression above the vacancy loop. Although such gaps in heavily strained parts of the crystal are understandable in terms of a rigid-shell model, they do not appeal to the intuition of the field-ion microscopist. In a real image these gaps would probably be closed (at least those in fig. 2), although possibly imaging at a lower intensity. Another problem is the occurrence of spurious image spots, close to the points of emergence of dislocations as, for example, in fig. 3 (*c*) (see also Stolt 1973). These difficulties in the use of computer simulation arise from the rigidity of the shell—lattice points are either inside it or outside, and the possibility of preferential field evaporation in heavily strained regions is not included in the model.

The strong shear stresses acting in certain parts of the tip (Smith *et al.* 1973) will affect the image contrast of loops in such regions. Although the stress cannot displace a Frank loop it will distort the strain field surrounding the loop and hence the contrast. The qualitative difference between vacancy and interstitial loops should not be smeared out by this, however.

In the discussion of perfect prismatic loops the effect on the dislocation of image forces due to the surface was not considered. It appears inconceivable however, that field evaporation through a perfect prismatic loop could occur without causing a part of it to glide out suddenly during the process. Unless pinned, the configuration of a perfect prismatic loop is determined by the balance between the acting shear stress and the line tension of the loop. When the tip surface approaches such a loop this balance is disturbed, the loop being attracted to the surface by the image force. Two cases may be envisaged. (1) Only the leading edge of the loop glides out first, causing a dipole to appear in the image; on further field evaporation, the rest of the loop glides out so that the dipole image disappears. (2) The whole loop glides out as soon as it begins to move. Since Frank loops are sessile, it is more likely to be possible to field-evaporate through an entire Frank loop without any sudden rearrangement of the configuration. It is thus possible that only Frank loops are capable of displaying contrast while intersecting the surface, since other kinds of loop would glide out of the tip before this contrast appears. Stable closed Shockley loops, as reported by Fortes and Ralph (1968), are hard to envisage; glide loops, if somehow nucleated, should either shrink under their own line tension or grow indefinitely under an acting shear stress. The stress acting on one of the loops reported by Fortes and Ralph (1968) has been computed by Smith *et al.* (1973), who found it to be $\mu/900$, where μ is the shear modulus, and concluded that this was consistent with the observation of the loops. It should be noted, however, that Smith *et al.* (1973) examined only the conditions for growth of the loop while the possibility of shrinkage apparently was not considered. A glide loop in the size range 20–100 Å will shrink unless acted on by a shear stress of at least $\mu/100$†. It therefore appears that only prismatic loops need be considered as causes of field-ion image contrast.

---

† A circular glide loop of radius r acted on by a shear stress τ will shrink unless $\tau b \geq S/r + \gamma$, where S is the line tension (Hirth and Lothe 1968, eqns. (6–45), and (6–68)) and γ is the stacking fault energy.

ACKNOWLEDGMENTS

The authors are grateful for the financial support of the U.S. Energy Resources and Development Administration through the Molecular and Materials Research Division of the Lawrence Berkeley Laboratory. Any conclusions or opinions expressed in this report are those of the authors alone and are not necessarily those of the Lawrence Berkeley Laboratory nor of the U.S. Energy Research and Development Administration.

REFERENCES

BOWKETT, K. M., and SMITH, D. A., 1970, *Field Ion Microscopy* (North-Holland).
FORTES, M. A., 1970, *Phil. Mag.*, **22**, 317.
FORTES, M. A., and RALPH, B., 1968, *Phil. Mag.*, **18**, 787.
HIRTH, J. P., and LOTHE, J., 1968, *Theory of Dislocations* (McGraw-Hill).
HREN, J. J., 1969, *Applications of Field-Ion Microscopy in Physical Metallurgy and Corrosion*, edited by R. F. Hochman, E. W. Muller and B. Ralph (Georgia Institute of Technology), p. 87.
MOORE, A. J. W., 1962, *J. Phys. Chem. Solids*, **23**, 907.
NEWMAN, R. W., and HREN, J. J., 1971, *Met. Trans.*, **2**, 1129.
PASHLEY, D. W., 1965, *Rep. Prog. Phys.*, **28**, 291.
PERRY, A. J., and BRANDON, D. G., 1968 a, *Phil. Mag.*, **17**, 255 ; 1968 b, *Ibid.*, **18**, 353.
RALSTON, A., 1965, *A First Course in Numerical Analysis* (McGraw-Hill).
RANGANATHAN, S., 1966, *J. appl. Phys.*, **37**, 4346 ; 1969 a, *Applications of Field-Ion Microscopy in Physical Metallurgy and Corrosion*, edited by R. F. Hochman, E. W. Muller and B. Ralph (Georgia Institute of Technology), p. 51 ; 1969 b, *Phil. Mag.*, **19**, 415.
RANGANATHAN, S., and DURAIRAGHAVAN, N., 1969, *Trans. Ind. Inst. Metals*, **22**, 6.
SANWALD, R. C., and HREN, J. J., 1968, *Surf. Sci.*, **9**, 257.
SMITH, D. A., BIRDSEYE, P. J., and GORINGE, M. J., 1973, *Phil. Mag.*, **27**, 1175.
SMITH, D. A., FORTES, M. A., KELLY, A., and RALPH, B., 1968, *Phil. Mag.*, **17**, 1065.
SMITH, D. A., MORGAN, R., and RALPH, B., 1968, *Phil. Mag.*, **18**, 869.
SON, U. T., and HREN, J. J., 1970, *Phil. Mag.*, **22**, 675.
STOLT, K., 1973, Ph.D. Thesis, University of California, Berkeley, Lawrence Berkeley Laboratory Report Number 2200.

This report was done with support from the United States Energy Research and Development Administration. Any conclusions or opinions expressed in this report represent solely those of the author(s) and not necessarily those of The Regents of the University of California, the Lawrence Berkeley Laboratory or the United States Energy Research and Development Administration.

TECHNICAL INFORMATION DIVISION
LAWRENCE BERKELEY LABORATORY
UNIVERSITY OF CALIFORNIA
BERKELEY, CALIFORNIA 94720